JMEPEG (2012) 21:2244–2254
DOI: 10.1007/s11665-012-0180-9
©ASM International
1059-9495/$19.00

Predictions of the Mechanical Properties and Microstructure Evolution of High Strength Steel in Hot Stamping

Junjia Cui, Chengxi Lei, Zhongwen Xing, Chunfeng Li, and Shumei Ma

(Submitted July 9, 2011; in revised form February 1, 2012)

Hot stamping is an innovative operation in metal-forming processes which virtually avoids the cracking and wrinkling of high strength steel (HSS) sheets. Examining the phase transformation and mechanical properties of HSS by means of experiments is challenging. In this article, a numerical model of the hot stamping process including forming, quenching, and air cooling was developed to reveal the microstructure evolution and to predict the final mechanical properties of hot-stamped components after multi-process cycles. The effects of the number of process cycles and the holding times on the temperature of HSS were examined using the model. The microstructure evolution of HSS under variable holding times is illustrated. The mechanical properties, particularly hardness and tensile strength, were predicted. It was found that the martensitic content increased with increasing holding time, and the martensitic content of the formed component at the flange and end was higher than for the sidewall, and lowest for the bottom. The hardness trend was consistent with the martensitic content. After six process cycles, the predictive errors of the model for hardness and tensile strength were acceptable for practical applications in engineering. Comparison between the predicted results and the experiment results showed that the developed model was reliable.

Keywords high strength steel, hot stamping, mechanical properties, microstructure

1. Introduction

High strength steel (HSS) can contribute to weight reduction in cars while maintaining safety standards and thus save fuel. However, the large springback and hard shape controllability create difficulties in the cold stamping of HSS for use in the automobile industry (Ref 1-5). As an innovative forming process for metal sheet, hot stamping, with integrated heating, forming, and quenching in one process, can effectively soften the blank and prevent it from cracking and wrinkling. Because of the phase transformation of austenite to martensite within the stamping operation, the blank can acquire substantial high tensile and yield strength (Ref 6, 7).

Phase transformations are inevitably involved due to rapid cooling of an austenized work piece in the hot stamping process (Ref 8). In general, the phase transformations in hot stamping are mainly affected by temperature distribution, and many factors can impact on temperature distribution such as the process cycles, holding time, and cooling medium. With so many influencing factors, the temperature distribution and microstructure evolution during the process are difficult to study using an experimental approach. Moreover, it is a time-consuming job to measure the mechanical properties of HSS after a hot stamping process. Therefore, accurate predictions of the microstructure evolution and mechanical properties of the hot-stamped component using the finite element method (FEM) are particularly useful. Over the past decade, several studies have considered phase transformations and mechanical properties for hot stamping analyses. For example, Åkerström certified that the models proposed by Kirkaldy can be used for simulating the phase transformations of many steels which have a total alloy content of approximately 2-3 wt.% without prior information from transformation diagrams (Ref 9). Bok et al. (Ref 10) proposed that a computer-aided design method incorporating phase transformation models be implemented, following thermomechanical-coupled finite element analysis, to predict the mechanical properties of hot formed components. In their FE analyses, the tools involved were usually modeled using thin shell elements, ignoring the effect of the cooling medium. Furthermore, their studies ignored the influence of process cycles. In general, the temperature of the tools increased with the number of process cycles, which resulted in a smaller cooling velocity of HSS, while the austenite, which would have transformed to martensite, began to transform to bainite. Therefore, a study on the process cycles should be made to provide guidelines for industrial production.

In this study, the FEM was used to develop a numerical model for multi-hot stamping process cycles of HSS. Using the model, we predicted the final mechanical properties and illustrated the microstructure evolution during the process. At the same time, the influences of process parameters such as the number of process cycles and the holding times on the

Junjia Cui and **Chunfeng Li**, School of Materials Science and Engineering, Harbin Institute of Technology, Harbin, China; **Chengxi Lei** and **Zhongwen Xing**, School of Mechanical Engineering, Harbin Institute of Technology, Harbin, China; and **Shumei Ma**, Institute of Crop Breeding, Heilongjiang Academy of Agricultural Sciences, Harbin, China. Contact e-mails: zoe122208@163.com, chxlei@126.com, gchxl@hit.edu.cn, lchfeng@hit.edu.cn and msm19@163.com.

mechanical properties and final microstructure of the hot-stamped component were investigated. The predicted results were compared with the results from the experiments to show the reliability of the developed model.

2. Experimental Procedures

HSS (BR1500HS) provided by the Baosteel Corporation was used as the work material for simulation, the chemical constituents of which are listed in Table 1. The thermophysical parameters under variable temperatures and the continuous-cooling-transformation curve of the material are described by Wang et al. (Ref 11). It was shown that cooling rates higher than 15 K/s result in a fully martensitic microstructure.

All stages of the hot stamping process are shown in Fig. 1. A boron-alloyed steel blank was heated in a furnace and austenized (Fig. 1a). The hot blank was then ejected from the furnace (Fig. 1b), formed by a deep drawing press (Fig. 1c), and subsequently quenched in the closed tools (Fig. 1d). The rapid cooling rate results in a transformation into martensite (Ref 12). After the quenching stage, the component is ejected from the tools and cooled by air (Fig. 1e).

The pipes are designed in the tools to provide the required cooling rate, usually to ensure a congruous cooling effect in the quenching stage. The experimental set-up for the hot stamping facilities, mainly including the die and punch, is shown in Fig. 2. The press has a maximum press force of 2000 kN with a die velocity of 100 mm/s. The furnace is a normal resistance type with a maximum heating temperature of 1200 °C.

Different locations, namely the end, bottom, flange, and sidewall, are selected for study areas, as shown in Fig. 3.

3. Finite Element Modeling

The hot stamping of sheet metal is a thermomechanical-forming process. The transformation from austenite into martensite causes an increase in volume, which influences the stress distribution during quenching (Ref 13). Therefore, the material model should be a temperature and strain-rate-dependent elastic-plastic model considering phase transformation and thermal expansion. The initial temperature of the blank and tools, and the phase transformation and thermal contact behavior between them, should be taken into account (Ref 14).

The thermomechanical-phase models of hot stamping were developed with the finite element software Deform 3D/HT®. The analysis was performed using a volume element for the blank and tools. The deformation of the tool and machine was neglected in the mechanical simulation of the hot stamping process.

Here, the modeling of forming, quenching, and cooling in the air was performed. The cooling of the hot blank in its transfer process from the furnace to the press was not considered in this study, and it was assumed that the blank had an initial homogeneous temperature of 860 °C due to free cooling from 950 °C during the transfer in the environment. An initial temperature of 20 °C for the tool and cooling water was prescribed.

Every process cycle was subdivided into two steps in the modeling and simulation of hot stamping. In the first step, a

Table 1 Chemical analysis of the investigated steel (in mass%)

C	Si	Mn	P	S	Cr	Ti	B	Al
0.2	0.4	1.2	0.02	0.015	0.25	0.04	0.002	0.04

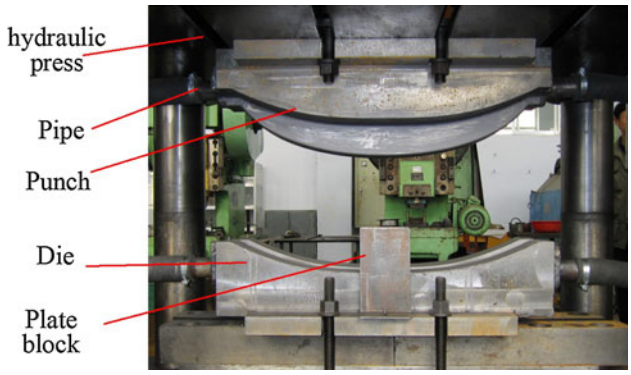

Fig. 2 The tools and cooling system

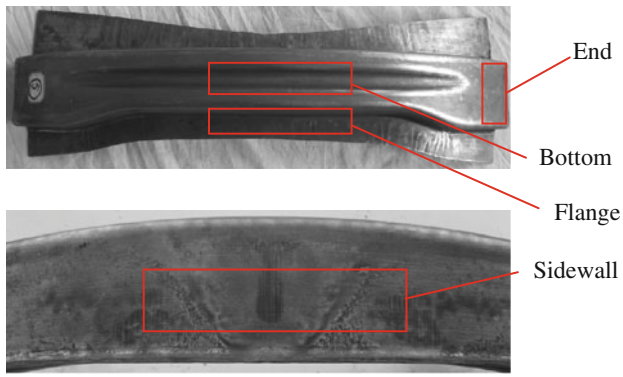

Fig. 3 Schematic of the study locations of deformed blanks

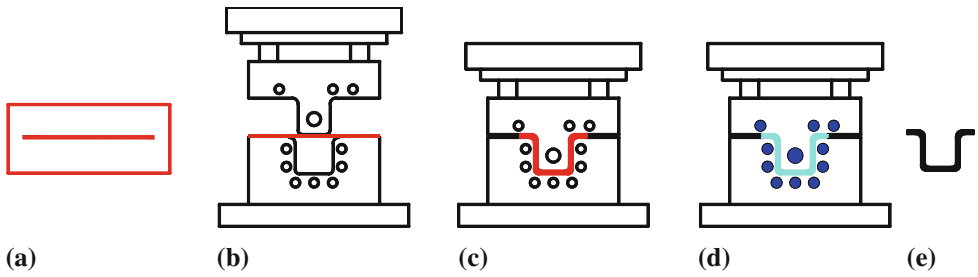

Fig. 1 Hot stamping process. (a) Heating, (b) locating, (c) stamping, (d) quenching in the tools, and (e) cooling in the air

blank was formed, quenched, and then cooled in the air. In the second step, when the blank was ejected from the tools, the water continued to cool the tools for some seconds until the next cycle started. According to the experiment, the temperature of the tools should reach a balanced state after six process cycles. Therefore, we analyzed the temperature, microstructure, and mechanical properties of HSS at the sixth process cycle to make the study useful to industrial production. Considering the symmetry of the hot stamping system, only half of the entire hot-forming system was modeled, as shown in Fig. 4. From the magnified window, we could see the tetrahedron element used to discretize the blank and tools, and the elements close to the tool surfaces were refined.

In this numerical model, a friction coefficient of 0.12 between blank and tools was used because the lubricant was graphite in the experiment and was assumed not to vary locally with interface temperature and pressure.

The flow stress data for the blank material obtained from tensile tests was used in the simulation (Fig. 5). The flow stress for the calculated strains, temperature, and strain-rate were logarithmically interpolated and extrapolated using the available input data (Ref 15).

Contact conditions considered in the thermal-mechanical-phase coupling analyses were (a) contact heat transfer between the blank and tools, (b) convection between the tools and pipes, and (c) radiation between the blank and the air.

According to Fourier's law, the heat transfer coefficient is affected by temperature and pressure (Ref 16). Equation 1 shows the heat transfer coefficient between HSS (22MnB5) and molded steel (Ref 17). The thermal parameters of the investigated material were similar to those of 22MnB5, so we assumed the equation was suitable for our study. It can be seen from Fig. 6 that the heat transfer coefficient increased with increasing pressure, because the higher the pressure, the better the contact state between the tools and blank. It was apparent that good contact between the blank and the tools facilitated heat transference from the blank to the tools.

$$h(p) = \frac{K\pi}{4\lambda}\left[1 + 85\left(\frac{p}{\sigma_r}\right)^{0.8}\right], \qquad \text{(Eq 1)}$$

where $h(p)$ is the heat transfer coefficient, K is the conductivity of air, λ is the roughness parameter, σ_r is the rupture stress, and p is the pressure.

In the analysis, the effect of the cooling medium was considered. The water was in a turbulent flow state with a

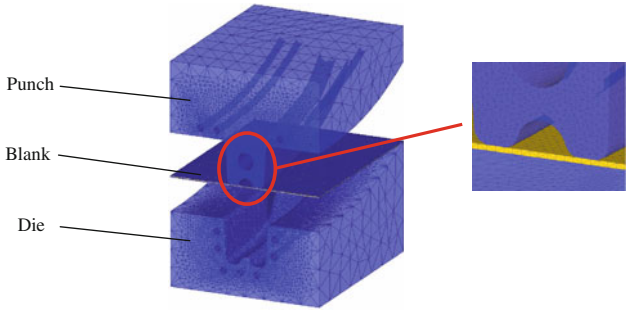

Fig. 4 Finite element models

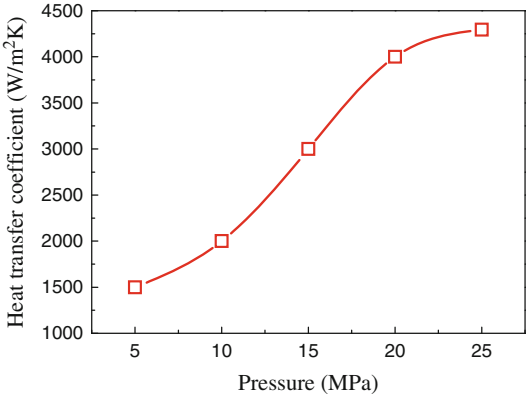

Fig. 6 Effect of pressure on heat transfer coefficient

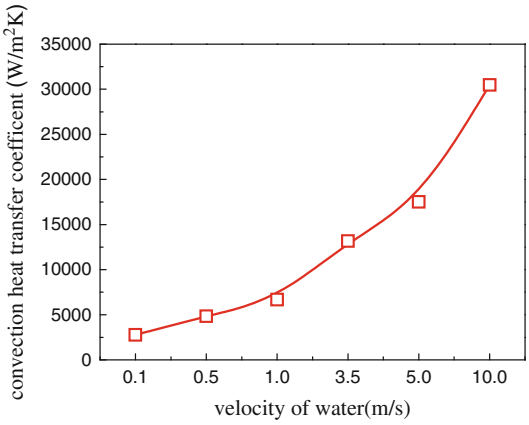

Fig. 7 Relationship between velocity of water and convection heat transfer coefficient

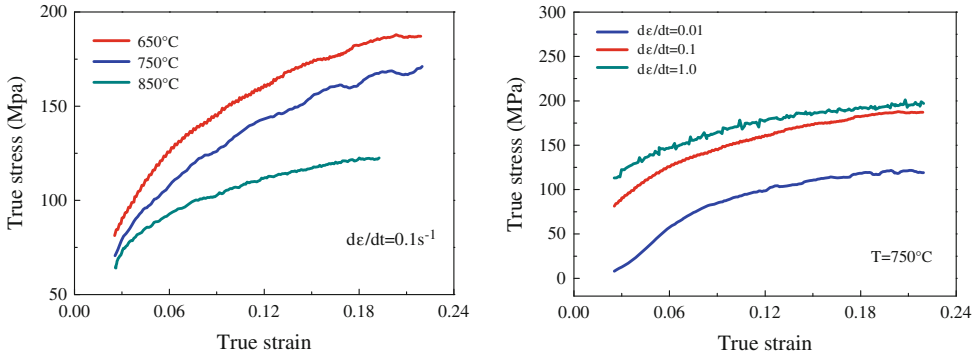

Fig. 5 Flow stress of BR1500HS at different temperatures and strain-rates

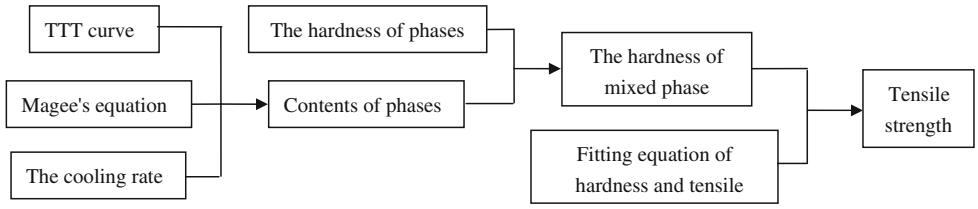

Fig. 8 The flow chart for mechanical properties prediction

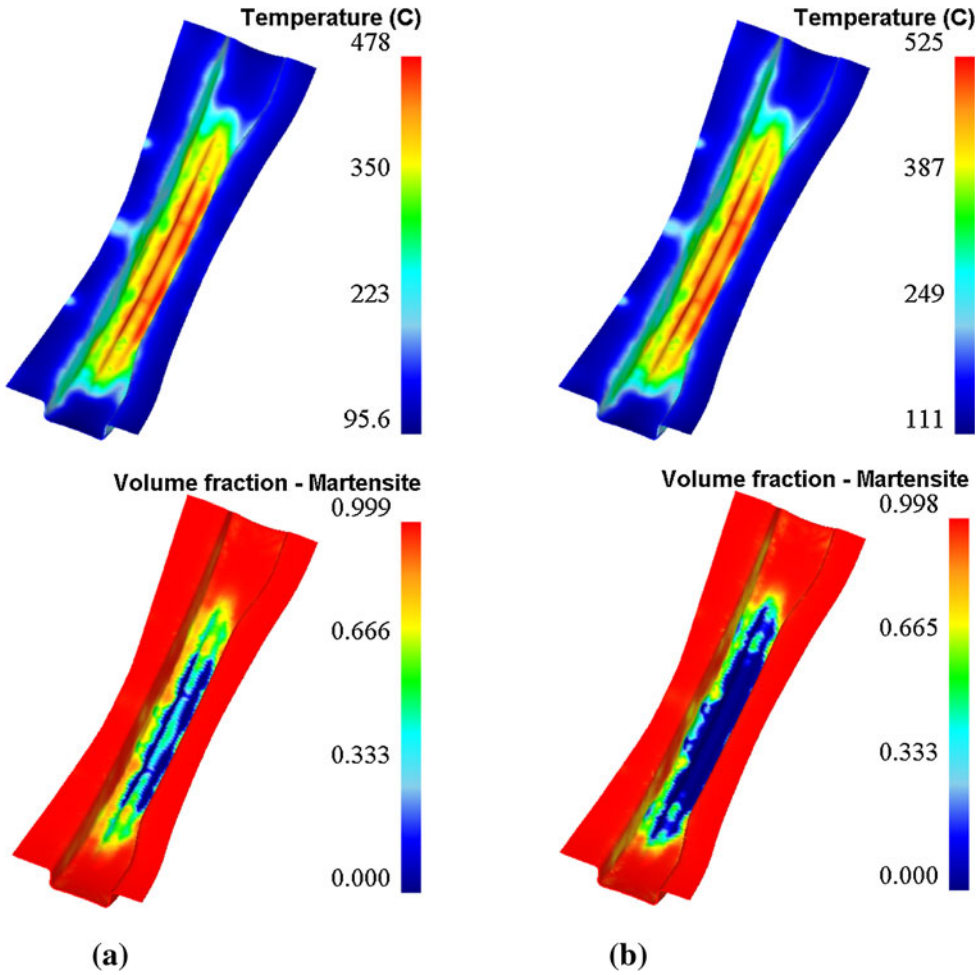

Fig. 9 Temperature and martensite distributions at the first (a) and the sixth (b) process cycles

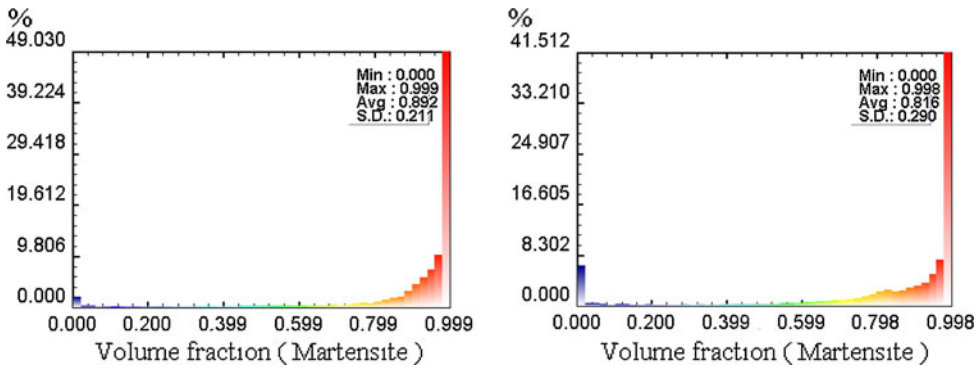

Fig. 10 Martensite statistical cloud of the formed blank at the first and the sixth process cycle

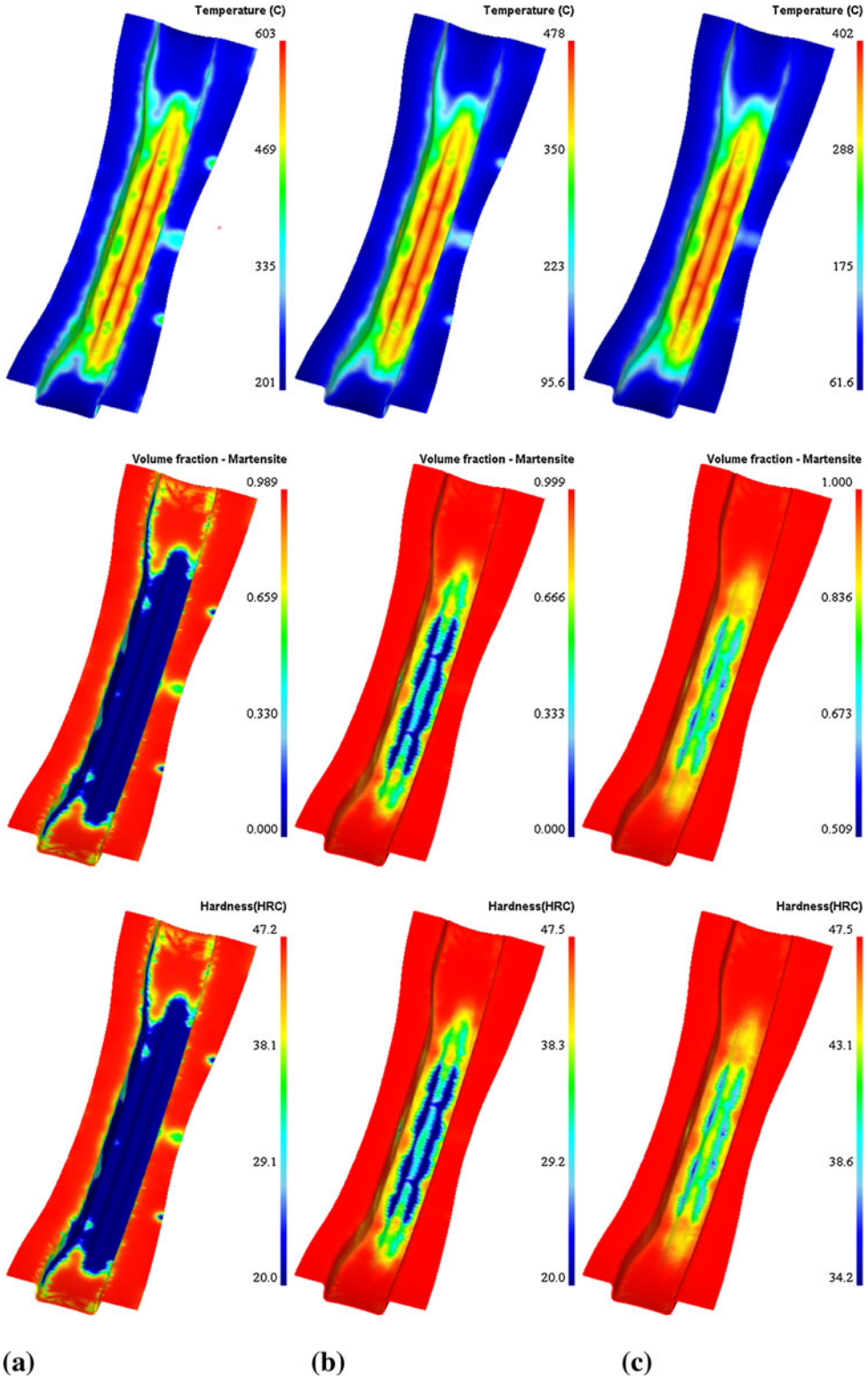

Fig. 11 Influence of holding times of 6 s (a), 10 s (b), and 13 s (c) on temperature, microstructure, and hardness distributions of the part at quenching process

Reynolds number of 2100, when it flowed at 3.5 m/s into the pipe of diameter 12 mm. Because of large temperature difference between the pipe wall and the water, the Sieder Tate Eq 2 was used to calculate the Nusselt number, which was the ratio of convective to conductive heat transfer across (normal to) the boundary at the boundary (surface) within a fluid (Ref 18).

$$N_{uD} = (0.027)R_{eD}^{0.8}p_r^{\frac{1}{3}}\left(\frac{u_b}{u_s}\right)^{0.14}, \quad \text{(Eq 2)}$$

where N_{uD} is the Nusselt number, R_{eD} is the Reynolds number, P_r is the Brandt number, u_b is the dynamic viscosity with average temperature, and u_s is the dynamic viscosity with surface temperature.

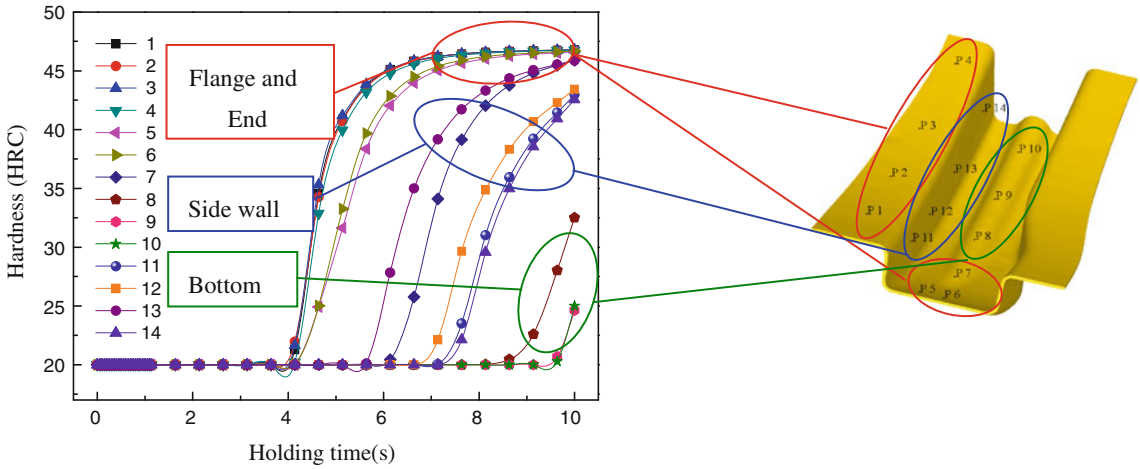

Fig. 12 Effects of holding time on hardness of different locations

The convection heat transfer coefficient was calculated by the following equation:

$$h = \frac{\lambda}{d} N_{uD}, \qquad \text{(Eq 3)}$$

where λ is the conductivity of water, d is the diameter, and N_{uD} is the Nusselt number.

The relationship between the velocity of water and the convection heat transfer coefficient is shown in Fig. 7, and was obtained by combining Eq 2 and 3. It illustrates that the increasing trend of the convection heat transfer coefficient will become more apparent with the increasing velocity of water. For the velocity of water 10 m/s, the convection heat transfer coefficient of 30481 W/m^{2}K was obtained.

Figure 8 gives the flow chart for predicting the mechanical properties. First, the cooling rates and temperature distributions of different domains of the specimen were calculated by the FEM. Using the cooling rates, temperature and TTT curve, the content of bainite was computed and we obtained the Magee parameters from the CCT curve to calculate the content of martensite using the Magee equation. Second, we set up the variable hardness of the phases in pre-processing which were obtained by experiment, giving the hardness of austenite, bainite, and martensite as 20 HRC, 40 HRC, and 50 HRC. The hardness of the mixed phase was calculated using the mixture algorithm together with the content of each phase. Finally, we carried out a quenching experiment to obtain the relationship between hardness and tensile strength, from which the tensile strength was predicted.

4. Results and Discussion

4.1 Effects of Process Parameters on the Temperature, Microstructure, and Hardness Distribution of HSS in the Hot Stamping Process

The two key factors of the phase transformation during hot forming are the process cycle and holding time with a fixed press and the convection heat transfer coefficient. The influences of the process cycle and holding time on the temperature and microstructure of HSS were investigated with a press of 2000 kN and a convection heat transfer coefficient of 30481 w/m^{2}k. Figure 9 shows the distributions of the temperature and microstructure of the formed component at the first and the sixth process cycle. The results illustrate that the temperature of the formed component increased with the increase in process cycles. The highest temperature increased from 478 to 525 °C, which caused the average martensite content to decrease from 89.2 to 81.6%, as shown in Fig. 10. The temperature and microstructure analyses are based on the sixth process cycle in the following.

Figure 11 shows the distributions for the temperature, microstructure, and hardness of the formed component under variable holding times at the sixth process cycle. The results show that the holding time had a significant influence on the distributions. The temperature of the formed component decreased with increased holding time, while the martensitic content and hardness increased. The martensitic content of the bottom of the formed component was the lowest, because the radial and tangential of the groove at the bottom of the formed component was created with a tensile stress at the beginning of the forming process, while it was subjected to compression stress in the axial direction at the end of the forming process. Both states of stress resulted in a thinning of the material, which lead to poor contact between the bottom and the punch, and a decrease in the heat transfer coefficient between the blank and the tools. The sidewall of the formed component cannot be cooled and quenched fully due to the die gap and small pressure, so the initial austenitic microstructure of the sidewall cannot be transformed into martensite completely at the end of quenching. The microstructure of the end and the flange was almost martensite at the end of quenching with a holding time of 10 s because of the large pressure and small die gap.

The hardness of the flange and end was more than 46 HRC with a holding time of 10 s, and that of the sidewall had lower values due to a smaller pressure and die gap, while the hardness of the bottom was the smallest because of the serious thinning.

The effects of holding time on hardness at several positions in different domains are illustrated in Fig. 12. According to the results, it was clear that the hardness of different zones increased markedly if the holding time increased to a certain value. The time at which hardness in different domains began to increase varied. For the flange and end it was 4 s, for the side wall 6 s, and the bottom 8 s. The dynamics of hardness in different locations was in accord with logarithmic growth.

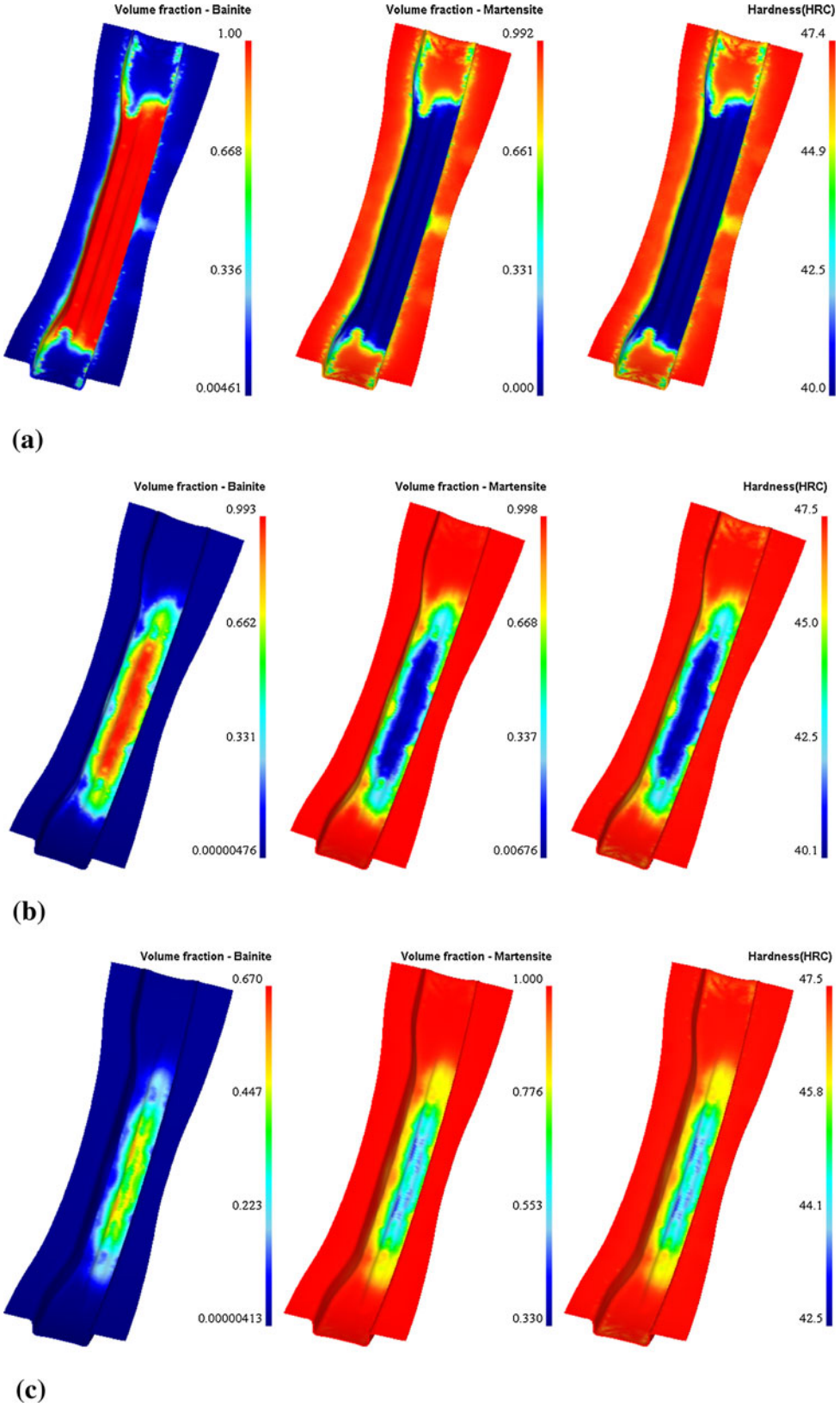

Fig. 13 Influence of holding times of 6 s (a), 10 s (b), and 13 s (c) on microstructure and hardness distributions of the part after air cooling process

After the quenching process, blanks were ejected from the dies and then cooled by air to room temperature. During this process, the heat of the blank was reduced by ambient air, and subsequently a slow temperature drop resulted in the bainite or other microstructure transformation. In fact, the experimental data were usually gathered at room temperature. Therefore, the

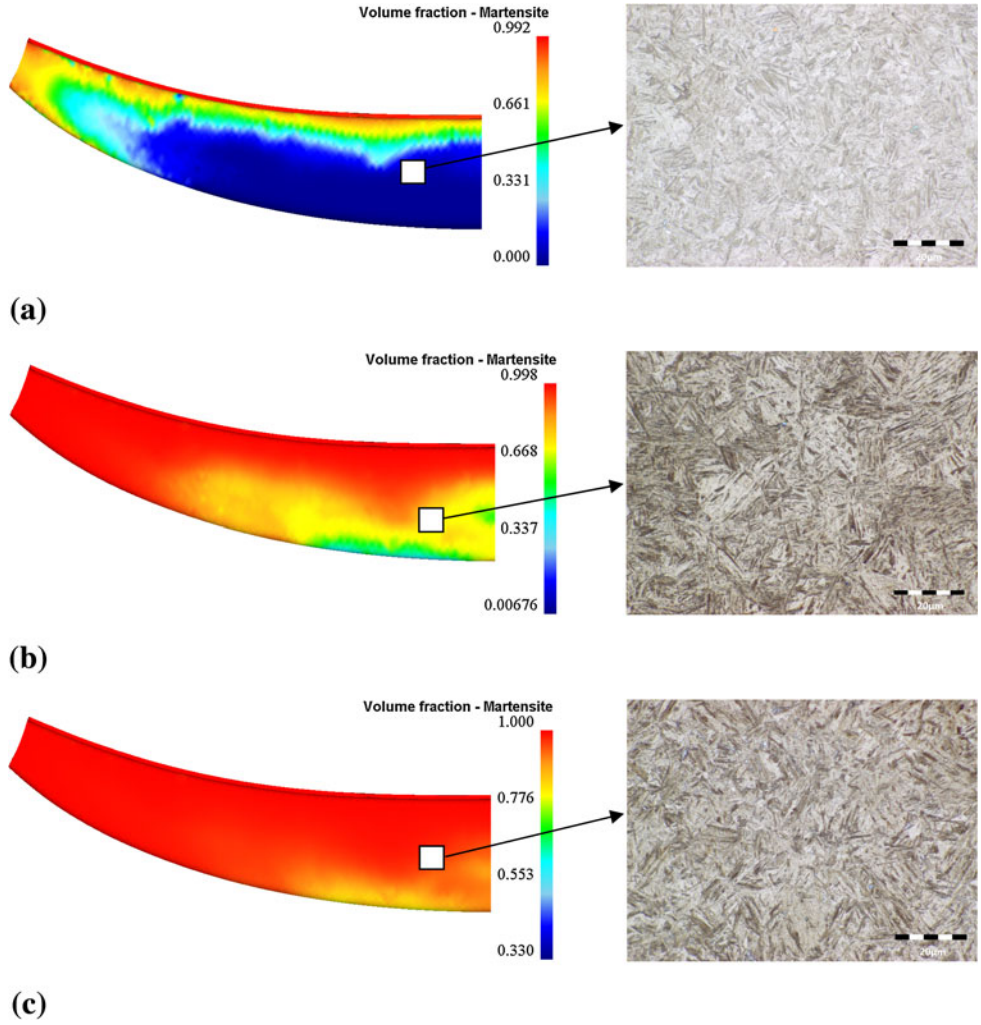

Fig. 14 Microstructure evolution of sidewall under variable holding times of 6 s (a), 10 s (b), and 13 s (c) after air cooling process

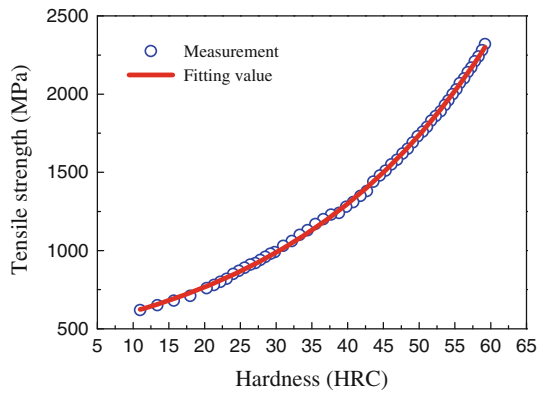

Fig. 15 Relationship between hardness and tensile strength

phase transformation behavior in the air cooling process was even more important. Predictions of hardness, microstructure, and tensile strength were also the aim of this process.

Microstructure and hardness distributions of the specimen after the air cooling process are given in Fig. 13. It can be seen that most of austenite located on the sidewall and bottom transformed to bainite as the holding time was below 10 s, while austenite transformed to martensite when the holding time was above 10 s. Martensite appeared mostly in the end and flange, and less in the bottom. Hardness corresponded to the martensitic content.

To reveal the microstructure evolution, we performed metallographic tests of a point on the sidewall under variable holding times, as shown in Fig. 14. As seen, the metallograph revealed that the martensitic content of the test point increased gradually as the holding time increased. Austenite mostly transformed to bainite with a holding time of 6 s after the air cooling process, and only a small amount of martensite began to appear, which corresponded with the simulation results. Most of austenite transformed to martensite with the holding time of 10 s. When the holding time reached 13 s, the microstructure of the sidewall mainly consisted of martensite. Meanwhile, it was also found that martensite appeared as a lath shape for the material, which is the reason for the high tensile strength of HSS under the hot stamping process.

4.2 The Prediction of Tensile Strength

4.2.1 Relationship Between Tensile Strength and Hardness. In this study, the experiments on the quenching process for BR1500HS were carried out to investigate the changes in hardness and tensile strength of the final product. Sheets with a thickness of 2 mm were austenitized at 950 °C for 5 min, and

then quenched in two different cooling media such as oil and water for different periods of time to obtain different microstructures.

Figure 15 shows the tensile strength and hardness of BR1500HS with different quenching process parameters. According to the results shown in Fig. 15, an increase in hardness improves tensile strength. Equation $y = y_0 + ae^{x/b}$ was applied to fit the curve by experiment, where y_0 = 226.05108, a = 272.0922, and b = 29.15449. The value of the correction coefficient of determination exceeded 0.999, which illustrates that hardness can be used to predict tensile strength.

4.2.2 Tests on the Mechanical Properties of BR1500HS. Tests on tensile strength and hardness were performed to study mechanical properties. The hardness tests were performed on the polished samples using the Rockwell hardness instrument.

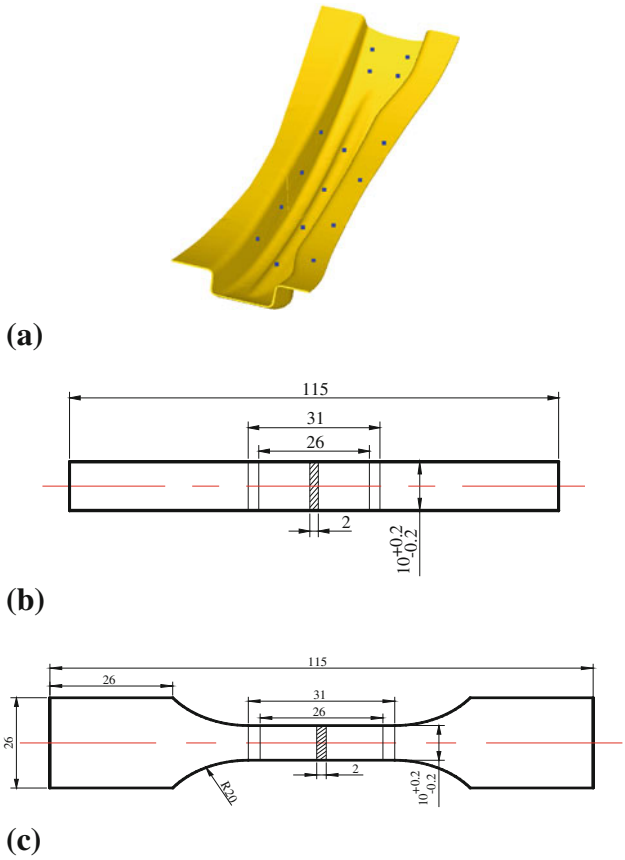

Fig. 16 Schematic of tensile test samples for end, flange, bottom (b), and sidewall (c) and positions of hardness tests (a)

Four points along the length were selected to evaluate the average values. The mechanical characteristics were determined using tensile tests for thin sheet metals at room temperature. Samples for determining tensile strength selected for different study areas were cut from the formed blank, as shown in Fig. 16. The geometry of the test samples was determined by the shape of the component. In the case of a formed component, the areas of the end, flange, and bottom were narrow and small, the standard samples were difficult to cut from these locations and, therefore, the ratio samples with rectangular shapes were used, whereas the space on the wall was considerable, so we chose a standard sample with a bone shape for the wall. For each test, two parallel specimens were examined. The mean values of the experimental and simulated hardness at the sixth process cycle are summarized in Table 2. It can be seen that the hardness increased gradually in different locations as the holding time extended, and the values of hardness at the end were higher than the others, while those at the bottom were the lowest. The distribution of hardness obtained by numerical simulation is consistent with that obtained by experiments.

The fitting equation established above was used to predict tensile strength, and the results are shown in Fig. 17. It can be seen from Fig. 17 that the variation tendency of the measured hardness in different domains was similar to the predicted values. With the holding time extended, the measured and the predicted hardness increased and the tensile strength of the hot-stamped samples varied from 1300 to 1500 MPa for a holding time exceeding 6 s. The tensile strengths of the end and flange were higher than in other positions, which can be more than 1500 MPa with a holding time exceeding 10 s, whereas that of the sidewall and bottom were the lowest, which coincided with the simulated results. With these values of tensile strength the hot-stamped components were listed in the range of ultra-HSSs.

The prediction errors of hardness and mechanical properties are shown in Fig. 18. As seen, the values of the prediction were higher than the actual values, because the uncoated steel generated a significant oxide layer during the forming process, which caused smaller heat transfer coefficients between the blank and the tools. In addition, the influence of the oxide layer on the flange was greater than in the other domains because there was no binder and the flange was exposed to the air for the longest time before the quenching stage, which resulted in errors with high values. In summary, the errors in the hardness of the sidewall and end were $<5\%$, and for strength were $<7\%$. Comparing the results for hardness, it was found that the simulation could correctly predict the tendency of the experiment, but the larger deflection of the sidewall shows some difference between the simulation and experiment. Further study will be required to improve the prediction accuracy for the air cooling process.

Table 2 Hardness of different locations of the blank under variable holding times at the sixth process cycle

	Measurement					Simulation			
Holding time	Sidewall	End	Flange	Bottom	Holding time	Sidewall	End	Flange	Bottom
6	39.2	42.7	41.0	36.6	6	40.5	45.8	44.3	39.0
8	40.1	44.3	43.3	37.9	8	42.9	46.0	46.1	40.1
10	42.2	44.7	43.7	41.6	10	43.0	46.2	46.2	41.5
13	43.1	45.1	44.6	43.5	13	45.3	46.4	46.4	44.6
16	44.6	45.3	45.4	43.6	16	46.2	46.4	46.5	45.2

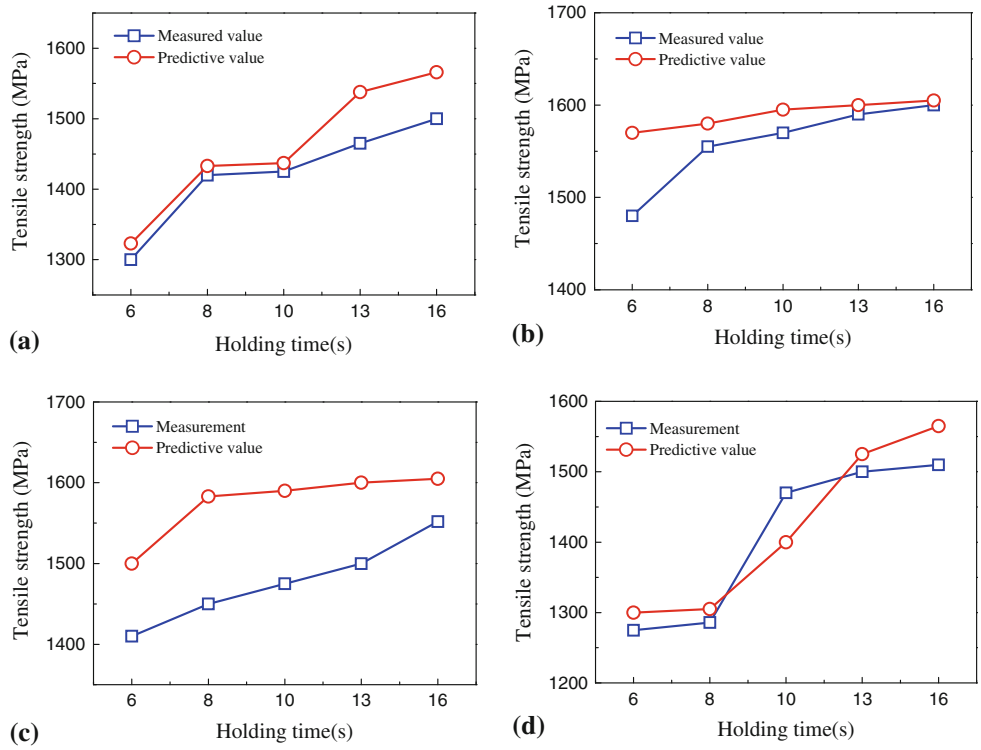

Fig. 17 Comparison between measurement and prediction in different locations of the specimen. (a) Sidewall, (b) end, (c) flange, and (d) bottom

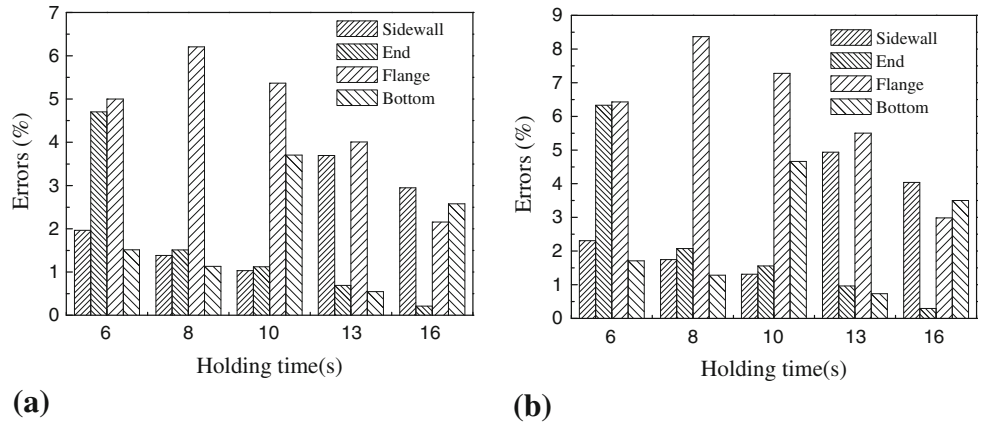

Fig. 18 Hardness (a) and tensile strength (b) errors in different locations of the specimen

5. Conclusions

An FE-coupled thermomechanical-phase model for predicting the final tensile strength and microstructure of a hot formed component was developed by carefully treating the complicated heat contact and heat conduction between the sheet and the tools. Numerical simulations of the hot stamping process were performed using the developed model. The influences of process cycles and holding time on the final microstructure and hardness of BR1500HS were investigated. Experiments for different quenching conditions were performed to establish the relationship between hardness and tensile strength. The phase transformation and mechanical properties of the HSS sheet were predicted by the experiments and the numerical simulations, and the following conclusions are drawn:

1. The hardness and martensitic content will be higher as the holding time increases, but lower as the process cycle decreases. To obtain a fully martensite microstructure, the holding time should exceed 10 s. In addition, pressure and gap play key roles in the quenching process, which results in different distributions of microstructure and hardness in the hot-stamped component.
2. From the quenching experiments on BR1500HS, the fitting equation, which describes the relationship between hardness and tensile strength, was established. The correction coefficient of the fitting equation was above 0.999, which illustrates that the tensile strength had a one-to-one correspondence relationship with hardness. Therefore, the tensile strength of a hot-stamped component can be predicted by hardness.

3. The numerical results including hardness and microstructure can be strongly influenced by serious oxidation of sheet metal. The predicted microstructure and hardness distributions during the quenching and air cooling process are in acceptable agreement with the experimental results.

References

1. A. Andersson, Numerical and Experimental Evaluation of Springback in Advanced High Strength Steel, *J. Mater. Eng. Perform.*, 2007, **16**, p 301–307
2. M. Naderi, V. Uthaisangsuk, U. Prahl, and W. Bleck, A Numerical and Experimental Investigation into Hot Stamping of Boron Alloyed Heat Treated Steels, *Steel Res. Int.*, 2008, **79**(2), p 77–79
3. A. Yanagida, T. Kurihara, and A. Azushima, Development of Tribo-simulator for Hot Stamping, *J. Mater. Process. Technol.*, 2010, **210**, p 456–460
4. T. Altan, Hot-Stamping Boron-Alloyed Steels for Automotive Parts, Part I: Process Methods and Uses, *Stamp. J.*, 2006, **40**, p 1–2
5. K. Mori and Y. Okuda, Tailor Die Quenching in Hot Stamping for Producing Ultra-High Strength Steel Formed Parts Having Strength Distribution, *CIRP Ann. Manuf. Technol.*, 2010, **59**, p 291–294
6. K. Kusumi, S. Yamamoto, T. Takeshita, and M. Abe, The Effect of Martensite Transformation on Shape Fixability in the Hot Stamping Process, *Steel Res. Int.*, 2008, **79**, p 71–76
7. P.F. Bariani, S. Bruschi, A. Ghiotti, and A. Turetta, Testing Formability in the Hot Stamping of HSS, *CIRP Ann. Manuf. Technol.*, 2008, **57**(1), p 265–268
8. M.-G. Lee, S.-J. Kim, and H.N. Han, Finite Element Investigations for the Role of Transformation Plasticity on Springback in Hot Stamping Process, *Comput. Mater. Sci.*, 2009, **47**, p 556–567
9. P. Åkerström and M. Oldenburg, Austenite Decomposition During Press Hardening of a Boron Steel—Computer Simulation and Test, *J. Mater. Process. Technol.*, 2006, **174**, p 399–406
10. H.-H. Bok, M.-G. Lee, E.J. Pavlina, F. Barlat, and H.-D. Kim, Comparative Study of the Prediction of Microstructure and Mechanical Properties for a Hot-Stamped B-Pillar Reinforcing Part, *Int. J. Mech. Sci.*, 2011, **53**, p 744–752
11. Li Wang, X-f Yang, and J-x Lu, Development of High Strength Steel Blanks for Lightweight Automobile, *Iron Steel*, 2006, **41**, p 5–7
12. D-l Song and S-h Jiao, Validation of Hardness Prediction Mathematic Models, *Mater. Mech. Eng.*, 2008, **32**(3), p 29–31
13. H. Karbasian and A.E. Tekkaya, A Review on Hot Stamping, *J. Mater. Process. Technol.*, 2010, **210**, p 2103–2118
14. M. Eriksson, M. Oldenburg, M.C. Somani, and L.P. Karjalainen, Testing and Evaluation of Material Data for Analysis of Forming and Hardening of Boron Steel Components, *Modell. Simul. Mater. Sci. Eng.*, 2002, **10**, p 1–18
15. J. Bao, H.-s. Liu, Z.H.-w. Xing, B.-y. Song, and Y.-y. Yang, Flow Behavior of Boron Steel for Hot Stamping at Elevated Temperature, *Mater. Sci. Technol.*, 2010, **18**(1), p 48–51
16. H.-s. Liu, W. Liu, J. Bao, and Z.H.-w. Xing, Numerical and Experimental Investigation into Hot Forming of Ultra High Strength Steel Sheet, *J. Mater. Eng. Perform.*, 2011, **20**(1), p 1–10
17. I.T. Shvets, Contact Heat Transfer Between Plane Metal Surfaces, *Int. Chem. Eng.*, 1964, **4**(4), p 621
18. D. Pitts and L. Sissom, *Schaum's Outline of Theory and Problems of Heat Transfer*, 2nd ed., McGraw-Hill, New York, 1998, p 194–197